

Supplement of Biogeosciences, 14, 3743–3762, 2017  
<https://doi.org/10.5194/bg-14-3743-2017-supplement>  
© Author(s) 2017. This work is distributed under  
the Creative Commons Attribution 3.0 License.



*Supplement of*

## **A global hotspot for dissolved organic carbon in hypermaritime watersheds of coastal British Columbia**

**Allison A. Oliver et al.**

*Correspondence to:* Allison A. Oliver (aaoliver@ualberta.ca)

The copyright of individual parts of the supplement might differ from the CC BY 3.0 License.

## 1 **Supplemental Material**

### 2 **S1. Watershed and soil attributes**

#### 3 **S1.1 Extent of wetlands and lakes**

4           Estimates of lake and wetland cover were extracted from the Province of British  
5 Columbia Terrestrial Ecosystem Mapping (TEM) (Green, 2014; Gonzalez Arriola et al., 2015).  
6 The estimate of wetland cover is derived by combining the cover of nine ecosystem classes  
7 typically considered to have wet (hygric to subhydryc) to very wet (hydric) soils, including  
8 blanket bogs, bog woodlands, basin bogs, fens and swamps (Banner et al., 1993, MacKenzie and  
9 Moran, 2004). This metric omits the widespread bog forests of Calvert and Hecate Islands,  
10 which have very moist (subhygric) to wet soil moisture regimes (Banner et al., 1993) and are  
11 transitional between upland and wetland ecosystems. The TEM dataset has polygons containing  
12 up to three ecosystem classes, with no information on the location of classes within polygons.  
13 Where TEM a polygon was intersected by watershed boundaries, we assumed a homogenous  
14 distribution of ecosystem classes within the polygon. After summing the cover of wetlands in  
15 each watershed we calculated the percentage of land (watershed area less lakes) covered by  
16 wetlands.

#### 17 **S1.2 Soil sampling and depth predictions**

18           Soil data were collected at a total of 353 field sites. Of these sites, 322 were located at  
19 fixed distances along transects established using a conditioned latin hypercube sampling design  
20 (Minasny and McBratney, 2006). The transect method was adopted because access on this  
21 remote island is restricted, and it was not possible to visit all of the points identified in the  
22 original hypercube procedure. The effect was to have small clusters of points that were well -  
23 distributed and representative of the study area. At all sites, the thickness of organic horizons,

24 thickness of mineral horizons, and total soil depth to bedrock were recorded, along with  
25 observations needed for categorization according to the Canadian System of Soil Classification  
26 (Soil Classification Working Group, 1998) and the British Columbia terrain classification  
27 (Howes and Kenk, 1997), where mineral soil horizons have  $\leq 17\%$  organic C, while organic soil  
28 horizons have  $> 17\%$  organic C, as per the Canadian System of Soil Classification (Soil  
29 Classification Working Group, 1998). Boundaries between surface organic horizons and the  
30 underlying mineral soil were usually obvious, based on colour, consistence, and  
31 presence/absence of mineral grains, but for occasional ambiguous cases, grab samples were  
32 collected for laboratory determination of C content by a ThermoFischer Scientific Flash 2000  
33 CHNS analyser at the Ministry of Environment laboratory in Victoria, B.C. For some sites, total  
34 depth exceeded the reach of sampling tools, so recorded thicknesses were likely conservative.  
35 Data were also collected at an additional 31 sites that were located in previously established  
36 ecosystem inventory plots with the same soil attributes (Giesbrecht et al., 2015). In addition to  
37 field-sampled points, 40 sites with exposed bedrock (0cm soil depth) were located using aerial  
38 photography.

39 Total organic horizon thickness, total mineral horizon thickness, and total soil depth were  
40 combined with a suite of topographic, vegetation, and remote sensing data for each sampling  
41 point, and the resulting dataset was used to train a random forest model (randomForest package  
42 in R; Liaw and Wiener, 2002) which predicted soil depth values and soil/terrain types for all  
43 points on the landscape. Depth predictions represent a modification of the procedure used by  
44 Scarpone et al. (2016) for depth predictions in interior British Columbia.

## 45 **S2. Hydrology- Rating curve calculations of stream discharge and error analysis**

### 46 **S2.1 Stage Measurements**

47 Stations were installed in the spring and early fall of 2014 as part of a telemetry network  
48 allowing for near real time download of data. At each station, an OTT PLS – L (OTT 2016)  
49 pressure transducer (0 - 4 m range SDI-12) was installed. Each sensor was connected to a  
50 CR1000 (Campbell Scientific, 2015) data logger. Stage measurements were recorded every five  
51 minutes with a five second sampling interval and mean, max, min and standard deviation of  
52 stream stage recorded over each five minute period. Each watershed also had stand-alone  
53 Odyssey Capacitance Water Level recorder (Data Flow Systems PTY Ltd 2016) installed in  
54 proximity to the pressure transducer to act as a back-up in case of sensor or data logger  
55 malfunction.

## 56 **S2.2 Discharge Measurements**

57 Stream discharge was measured using multiple methods. Low and moderate flows,  
58 generally below  $0.5 \text{ m}^3 \text{ s}^{-1}$ , were measured using the velocity area method midsection discharge  
59 equation (ISO, 1992; ISO, 1997). The flow velocities were measured with the Swoffer 2100  
60 propeller type mechanical current meter (Swoffer Instruments Inc., Seattle, USA) or the Sontek  
61 Flowtracker acoustic doppler velocimeter (SonTek, San Diego, USA). Flow velocities were  
62 averaged by the Swoffer over a five second measurement interval and by the Flowtracker over a  
63 30 second measurement interval for each location. A suitable river cross-section site was defined  
64 by: a) general flow direction perpendicular to the cross-section line, b) uniform stream bed  
65 conditions, and c) constrained flow conditions with no back eddies and low turbulence.  
66 At some watersheds, multiple velocity-area sites were used depending on conditions at time of  
67 measurement.

68 At flows greater than  $0.5 \text{ m}^3 \text{ s}^{-1}$ , salt dilution was the primary method to measure  
69 discharge, specifically salt in solution (“salt solution”) as described by Moore (2005). Discharge  
70 was calculated using the following formula:

$$71 \quad Q = \frac{V}{\sum RC_t \cdot t_{\text{int}}} \quad (4)$$

72 where V represents the volume of salt solution ( $\text{m}^3$ ),  $RC_t$  the relative concentration of salt  
73 solution ( $\text{mL mL}^{-1}$ ) and  $t_{\text{int}}$  is the time interval of measurement.  $RC_t$  is obtained using a relative  
74 concentration, related to electrical conductivity (EC):

$$75 \quad RC_t = (EC_t - EC_0) \cdot CF \quad (5)$$

76 where  $EC_t$  is the temperature corrected EC measured at time t ( $\mu\text{S cm}^{-1}$ ),  $EC_0$  is the baseline  
77 conductivity of the stream ( $\mu\text{S cm}^{-1}$ ) defined as the five minute average prior to the salt wave,  
78 and CF is the calibration factor. The end of the salt wave was defined as the point in which the  
79 five minute EC average equaled  $EC_0$ . In some instances the post-five minute average would not  
80 return to  $EC_0$  due to changes in background chemistry not associated with the salt dump. When  
81 this occurred,  $EC_0$  was determined by linear interpolation for baseline EC, pre and post  
82 measurement.

83 The CF is defined as the relationship between additions of primary solution (made up of  
84 salt solution and stream water) to a known volume of secondary solution (stream water only),  
85 with the resulting slope of the line corresponding to the CF value. The primary solution was  
86 typically made up of 10 mL salt solution (used in discharge measurement) added to 1000 mL of  
87 stream water. Then, 2 or 5 mL increments of the primary solution was pipetted into 3000 mL of  
88 the secondary solution, and corresponding changes in EC were recorded. Linear regression was  
89 performed to determine slope of the line.

90           Due to difficulties associated with being on location to measure high discharge, a “salt  
91 dilution system” was designed using the salt solution method described above. The system was  
92 entirely automated and located within an extensive telemetry network enabling remote activation  
93 off-site or through pre-programmed stream stages where discharge measurements had not been  
94 previously measured.

95           A volume of salt solution, stored in two, 200 L barrels on site, allowed for up to thirty  
96 measurements between refills. Recharging of the salt solution reservoir was done manually and  
97 the CF completed following the refill and prior to the next refill (the reservoir was designed to  
98 ensure that at least 5 L of solution remained after the final discharge measurement), for a  
99 minimum of two CF’s between refills. When the water level reached a predefined stage, a signal  
100 was sent to release a pre-determined volume of salt solution from a reservoir connected to the  
101 salt solution storage barrels. To increase the accuracy of this volume, the salt solution was first  
102 pumped into a stainless steel cylinder with a pressure transducer at the bottom to measure water  
103 depth, and in turn volume. The solution was then transferred to a dumping mechanism located  
104 above the stream designed for near instantaneous release. Upon initiation of the salt solution  
105 dump sequence, a second command was sent to a downstream data logger to activate two Global  
106 Water-WQ Cond sensors (Global Water instrumentation, Inc., College Station, USA) to measure  
107  $EC_t$  at one second intervals, and therefore capture the passing salt wave. Once the dump  
108 sequence was completed, the  $EC_t$  data were transmitted via the telemetry network to a server  
109 accessed via the internet. The volume of salt depended on estimated discharge measurements,  
110 with maximum EC measurements targeted to be no more than 40 uS above background, well  
111 below the most sensitive toxicity threshold of 400 mg L<sup>-1</sup> (Moore 2004a, 2004b).

### 112 **S2.3 Error and uncertainty analysis**

113 **S2.3.1 Discharge measurement error analysis**

114 Errors associated with manual direct discharge measurements were estimated using  
115 statistical techniques and on-site observations. For the velocity-area method, discharge  
116 uncertainty was calculated using the Interpolated Variance Estimator (IVE) (Cohn et al., 2013).  
117 For the salt dilution method, a statistical and site specific uncertainty estimation method was  
118 developed.

119 **S2.3.2 Uncertainty analysis for the velocity-area measurements**

120  
121 As described in Cohn et al. (2013), the IVE was used to estimate uncertainty in velocity  
122 area discharge measurements. It is based on the assumption that depth and velocity vary  
123 gradually across a channel cross-section and that depth and velocity vary linearly between  
124 adjacent stations. The difference between the assumed and the measured value is used to  
125 calculate measurement uncertainty. In addition, uncertainties associated with calibration and  
126 systemic errors in the width, depth, and velocity were assumed to be 1% for the Sontek  
127 Flowtracker (the accuracy of the device calibration; Sontek/YSI, 2007) and 5% for the Swiffer  
128 current meter, due to increased potential uncertainty from the shorter time interval used to  
129 determine average velocity. Total uncertainty was estimated based on the above uncertainties  
130 and the number of measurement stations (see Cohn et al. 2013).

131 **S2.3.3 Salt dilution discharge uncertainty**

132  
133 The discharge uncertainty for salt dilution measurements was estimated using the  
134 sensor resolution, calibration errors, salt volume errors, and salt mixing errors. Uncertainty ( $u_Q$ ),  
135 associated with discharge calculated from a conductivity sensor is based on the following:

136 
$$u_Q = u_v + \frac{\sum_{i=1}^m ((u_{EC,i} + u_{CF})C_i)}{\sum_{i=1}^m C_i} \quad (6)$$

137

138 Where  $u_v$  is the relative uncertainty due to salt volume error (%),  $u_{EC,i}$  is the relative uncertainty  
139 in EC measurement  $i$  due to the resolution of the sensor (%),  $u_{CF}$  is the relative uncertainty in CF  
140 (%),  $C_i$  is the calculated salt concentration at measurement  $i$  ( $\text{g m}^{-3}$ ), and  $m$  is the total number of  
141 EC measurements.

142 Error associated with determining the volume of salt ( $u_v$ ) was estimated by:

$$143 \quad u_v = \frac{\Delta v}{v} \cdot 100 \quad (7)$$

144 where  $V$  is the volume of salt solution released to the stream (L), and  $\Delta V$  is the estimated error in  
145 salt solution volume (L). The error in solution volume was estimated based on the resolution (1  
146 mm) of the pressure transducer inside the stainless steel cylinder salt dump reservoir. With an  
147 uncertainty of 0.5 mm in solution height inside the cylinder and a cylinder diameter of 304 mm,  
148 the uncertainty in solution volume for each release was 36.3 mL. Because the cylinder was never  
149 completely emptied, two level measurements were made to calculate water, thus total maximum  
150 error in solution volume ( $\Delta V$ ) was 72.6 mL.  
151  
152

153 Electrical conductivity measurement uncertainty ( $u_{EC}$ ), dependent on the resolution of  
154 the conductivity sensor (Res) is described below:

$$155 \quad u_{EC} = \frac{0.5 \cdot \text{Res}}{EC} \cdot 100 \quad (8)$$

156  
157 Uncertainty related to  $u_{CF}$  was a function of the errors associated with the measurement  
158 of salt concentration of the primary and secondary solution, a combination of volumetric error of  
159 the primary solution ( $\pm 0.3$  mm, volumetric flask precision), the secondary solution ( $\pm 3.0$  mm  
160 volumetric flask precision plus rain splash and field conditions) and each primary solution dose  
161 (0.006 mL, based on precision of the pipette) added in 2 or 5 mL increments. Uncertainty of the  
162 CF was derived from the maximum variation in slope, a product of the salt concentration error  
163 ranges. The calibration regression curve was plotted using three data points for each conductivity

164 measurement: the assumed salt concentration, the assumed salt concentration plus maximum  
 165 error, and the assumed salt concentration minus maximum error (Figure S2.1). Next, the  
 166 maximum variation of slope was calculated using the standard deviation of slope ( $\sigma_s$ ):

$$167 \quad \sigma_s = \sqrt{\frac{(\frac{1}{n-2}) \sum_{i=1}^n (y_i - \hat{y}_i)^2}{\sum_{i=1}^n (x_i - \bar{x})^2}} \quad (9)$$

168 where n is the number of data points,  $y_i$  is the assumed salt concentration ( $\pm$  error) of  
 169 measurement i ( $\text{mL mL}^{-1}$ ),  $\hat{y}_i$  is the modelled salt concentration ( $\text{mL mL}^{-1}$ ),  $x_i$  is the measured  
 170 electrical conductivity of measurement i ( $\mu\text{S cm}^{-1}$ ), and  $\bar{x}$  is the mean average electrical  
 171 conductivity ( $\mu\text{S cm}^{-1}$ ). Finally, the CF relative uncertainty ( $u_{CF}$ ) was defined as two times the  
 172 standard deviation of slope divided by the CF:  
 173

$$174 \quad u_{CF} = (2 \cdot \sigma_s) / CF \quad (10)$$

175  
 176 If the EC sensors showed different EC readings and confirmed the salt was not  
 177 completely mixed at the measurement site, additional uncertainty was added to the discharge  
 178 measurement. To measure the degree of salt mixing at the measurement site, discharges  
 179 calculated from both conductivity sensor measurements were compared, while taking their  
 180 uncertainties into account:

$$181 \quad M = \frac{(Q2 - \epsilon_{Q2}) - (Q1 + \epsilon_{Q1})}{(Q1 + \epsilon_{Q1})} \cdot 100 \quad (11)$$

182 where M is the relative uncertainty due to improper mixing (%), Q1 is the lower discharge value  
 183 ( $\text{m}^3 \text{s}^{-1}$ ), Q2 is the higher discharge value ( $\text{m}^3 \text{s}^{-1}$ ),  $\epsilon_{Q1}$  is the absolute uncertainty of the lower  
 184 discharge value, derived from  $u_Q$  (Equation 6) and  $\epsilon_{Q2}$  is the absolute uncertainty of the higher  
 185 discharge value. If  $M \leq 0$ , the salt was assumed to be properly mixed. Any positive outcome of  
 186 M implies incomplete mixing and is added to the total uncertainty of the discharge measurement.  
 187

## 188 **S2.4 Rating curve development and uncertainty**

189  
190 Discharge is related to stage through the formula:

$$191 \quad Q = a(h - h_0)^b \quad (12)$$

192 where  $Q$  is discharge ( $\text{m}^3 \text{s}^{-1}$ ),  $h$  is stage level (m),  $h_0$  is the water level at zero flow (m) and  $a$  and  
193  $b$  are coefficients specific to the gauging station of a river. The values for  $h_0$ ,  $a$ , and  $b$  are  
194 obtained by the curve fitting results of simultaneous stage and discharge measurements. For this  
195 work, stage-discharge curves were created using a non-linear least-squares fitting Python model  
196 (lmfit; LMFIT Development Team, 2015). This model approximates the variables ( $a$ ,  $b$ , and  $h_0$ )  
197 by minimizing the residuals scaled by data uncertainties:

$$198 \quad [Q_i^{\text{meas}} - Q_i^{\text{model}}(v)]/\varepsilon_i \quad (13)$$

199 where  $Q_i^{\text{meas}}$  is the measured discharge ( $\text{m}^3 \text{s}^{-1}$ ),  $Q_i^{\text{model}}$  is the fitted discharge ( $\text{m}^3 \text{s}^{-1}$ ),  $v$  the set  
200 of variables in the model ( $a$ ,  $b$  and  $h_0$ ) to be optimized, and  $\varepsilon_i$  the uncertainty in the discharge  
201 measurement. This was a two step process where the curve was first fit taking into account  
202 uncertainties related to  $Q$  and then fit again taking into account uncertainties in  $h$ .

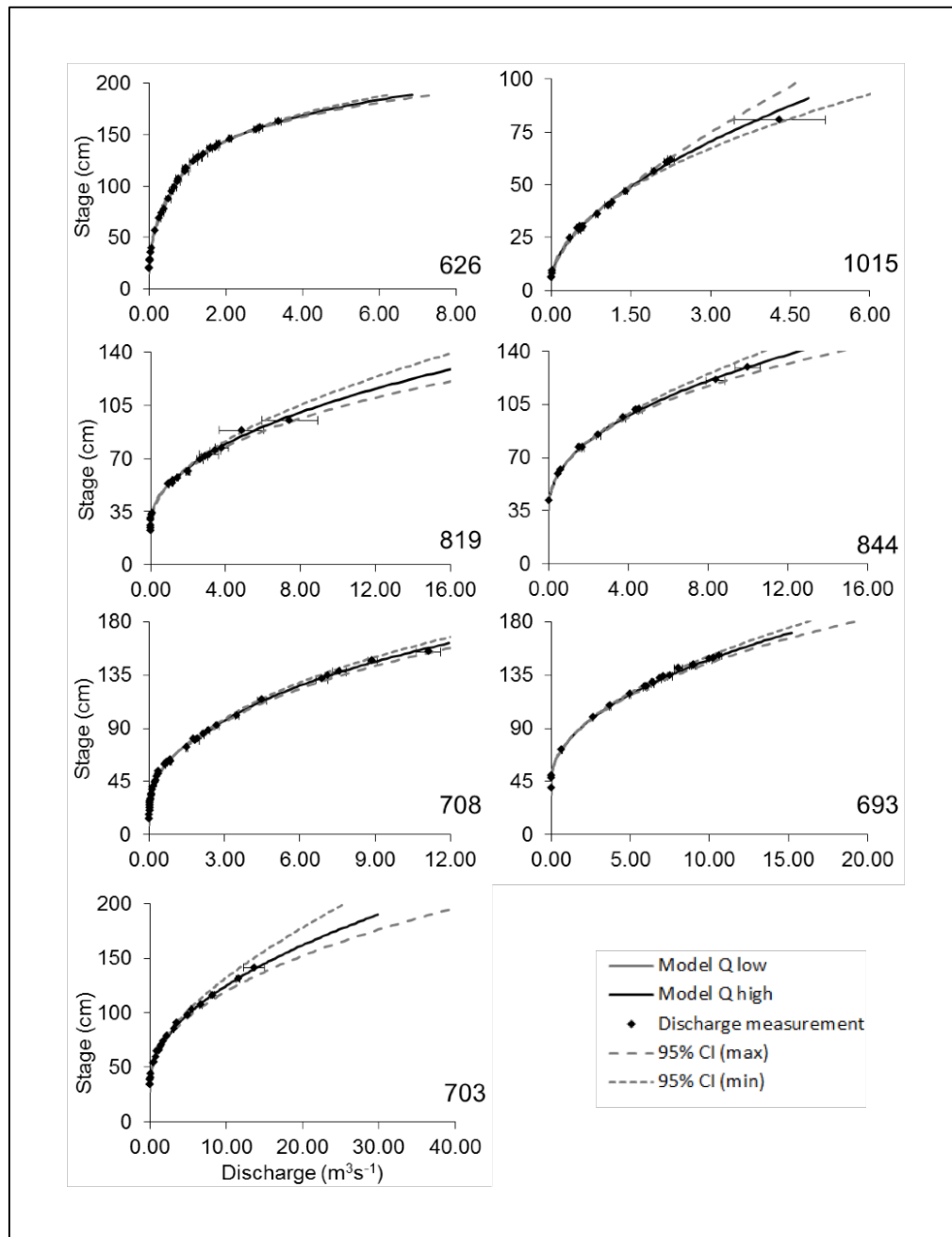
203 As described above, uncertainty for individual discharge measurements were accounted  
204 for in the curve fitting process, with measurements of greater uncertainty having less influence  
205 on position of the curve. To account for uncertainty in the stage discharge relation, 95%  
206 confidence intervals were created per Herschy (1994) and applied to the final discharge times-  
207 series as an estimate of discharge.

## 208 **S2.5 Results of stream discharge measurement and calculations**

209 A total of 168 total measurements, including 92 measures made using the automated  
210 system, were used to develop rating curves for each watershed (Figure S2.1; Floyd et al., 2016).  
211 Watershed 703 had the highest total discharge over the study period, which was more than the

212 combined total from watersheds 626, 819, 844 and 1015. Total discharge calculated from the  
213 95% confidence intervals from the rating curves were  $\pm 6.5\%$  of the mean of all watersheds, with  
214 a range between  $\pm 2.93\%$  (708) and  $\pm 9.98\%$  (819) (Table S2.3). In general, discharge data from  
215 watershed 708 had the lowest uncertainty, due to it having the most discharge measurements and  
216 the best developed rating curve. Watershed 819 had the highest uncertainty largely due to the  
217 limited number of high flow discharge measurements on the rating curve (max measured was  $4.5$   
218  $\text{m}^3\text{s}^{-1}$ ) and variation in stage during the discharge measurements at high flow. Four of the seven  
219 watersheds had total discharge measurements less than  $\pm 5.0\%$  of the estimated measurements  
220 from the rating curve, and none were  $> 10\%$  for the entire project study period, however for  
221 water year 2015/2016, 819 had a total discharge uncertainty of  $\pm 13.0\%$ .

222 **Figure S2.1.** Stage discharge rating curves for seven focal watersheds. Confidence intervals  
223 (95%) are calculated based on Herschy (1994). Error bars represent uncertainty from individual  
224 measurements.



225  
 226  
 227  
 228  
 229  
 230  
 231

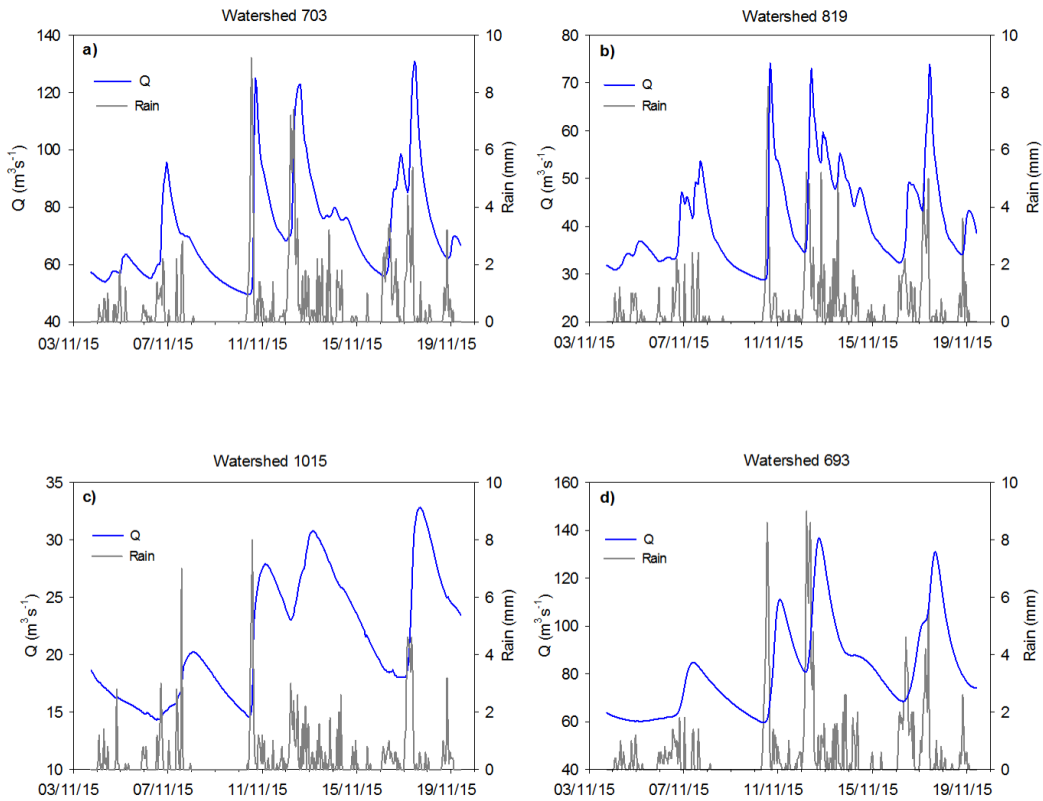
**Table S2.1.** Uncertainty (%) in total discharge, by water year and over the entire study period, based on rating curve confidence intervals (95%). Values are plus or minus the modelled output.

<i>Watershed</i>	<i>2014-15</i>	<i>2015-16</i>	<i>2014-2016</i>
626	5.57	5.54	5.55
693	3.35	2.97	3.19
703	10.14	9.37	9.83

708	2.93	2.93	2.93
819	7.49	13.01	9.98
844	4.98	4.47	4.78
1015	9.01	8.58	8.84

232  
233  
234  
235  
236  
237  
238  
239

**Figure S2.2:** Response times of watersheds with and without extensive lake area. Discharge and total precipitation are shown for a series of rain events in four of our seven focal watersheds. Panels “a” and “b” represent watersheds without extensive lake area, and panels “c” and “d” represent watersheds with a large lake area. Specific information on lake area can be found in the manuscript, Table 1. Rapid response to rain events can be observed in each watershed, while the falling limb of the hydrograph is delayed in systems with extensive lake area compared to those without.



240  
241  
242  
243  
244  
245  
246  
247

### S3. Generating model estimates of DOC flux using rloadest

**Table S3.1:** The number of samples and specific regression model used by rloadest for calculating stream loads. Estimated bias of each model shows relatively low overall bias for each model, with 844 clearly showing the highest bias.

Watershed	n	Model #	Regression model	Estimated % bias
626	23	7	$a_0 + a_1 \ln Q + a_2 \sin(2\pi dtime) + a_3 \cos(2\pi dtime) + a_4 dtime$	2.026
1015	24	7	$a_0 + a_1 \ln Q + a_2 \sin(2\pi dtime) + a_3 \cos(2\pi dtime) + a_4 dtime$	-2.502
819	23	7	$a_0 + a_1 \ln Q + a_2 \sin(2\pi dtime) + a_3 \cos(2\pi dtime) + a_4 dtime$	2.011
844	20	3	$a_0 + a_1 \ln Q + a_2 dtime$	-11.49
708	24	6	$a_0 + a_1 \ln Q + a_2 \ln Q^2 + a_3 \sin(2\pi dtime) + a_4 \cos(2\pi dtime)$	-0.206
693	23	6	$a_0 + a_1 \ln Q + a_2 \ln Q^2 + a_3 \sin(2\pi dtime) + a_4 \cos(2\pi dtime)$	0.092

248

249

250

251

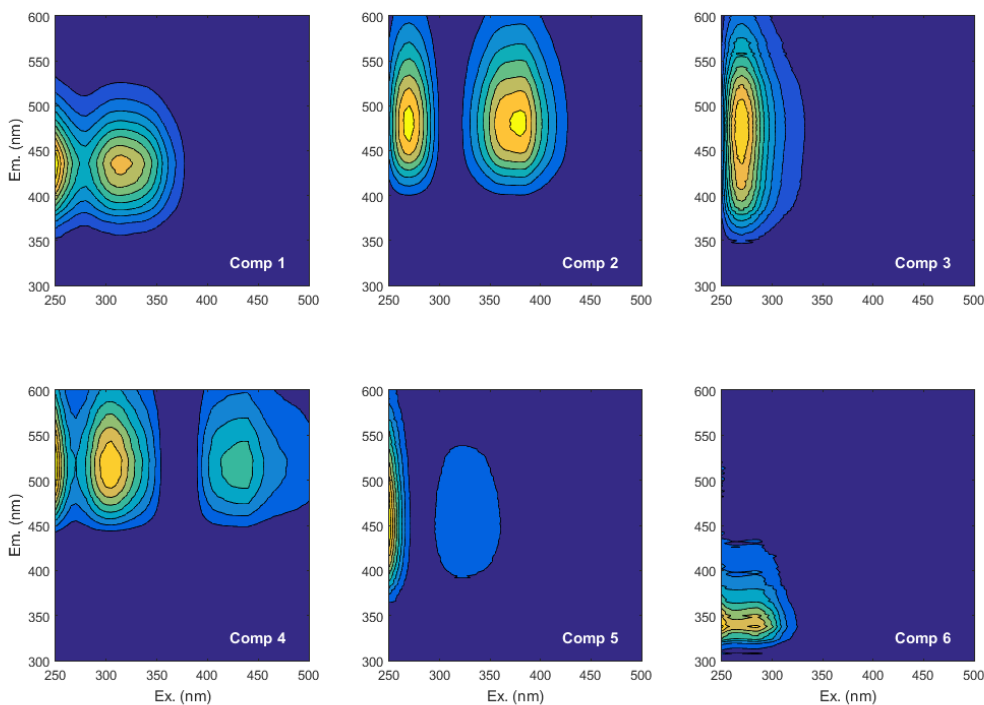
#### S4. PARAFAC Modeling of DOM composition

252

253

**Figure S4.2:** Fingerprint map showing the six fluorescence components determined by PARAFAC analysis.

254



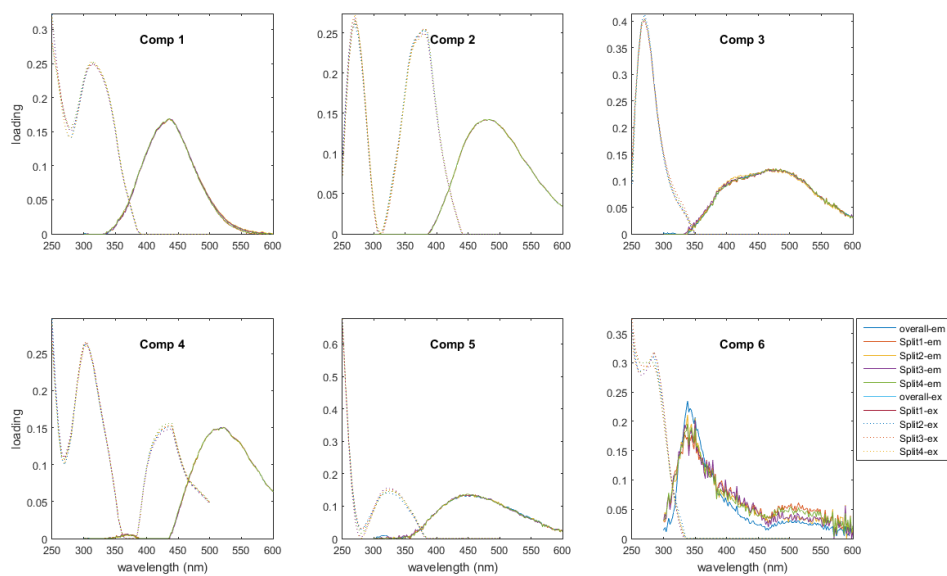
255

256

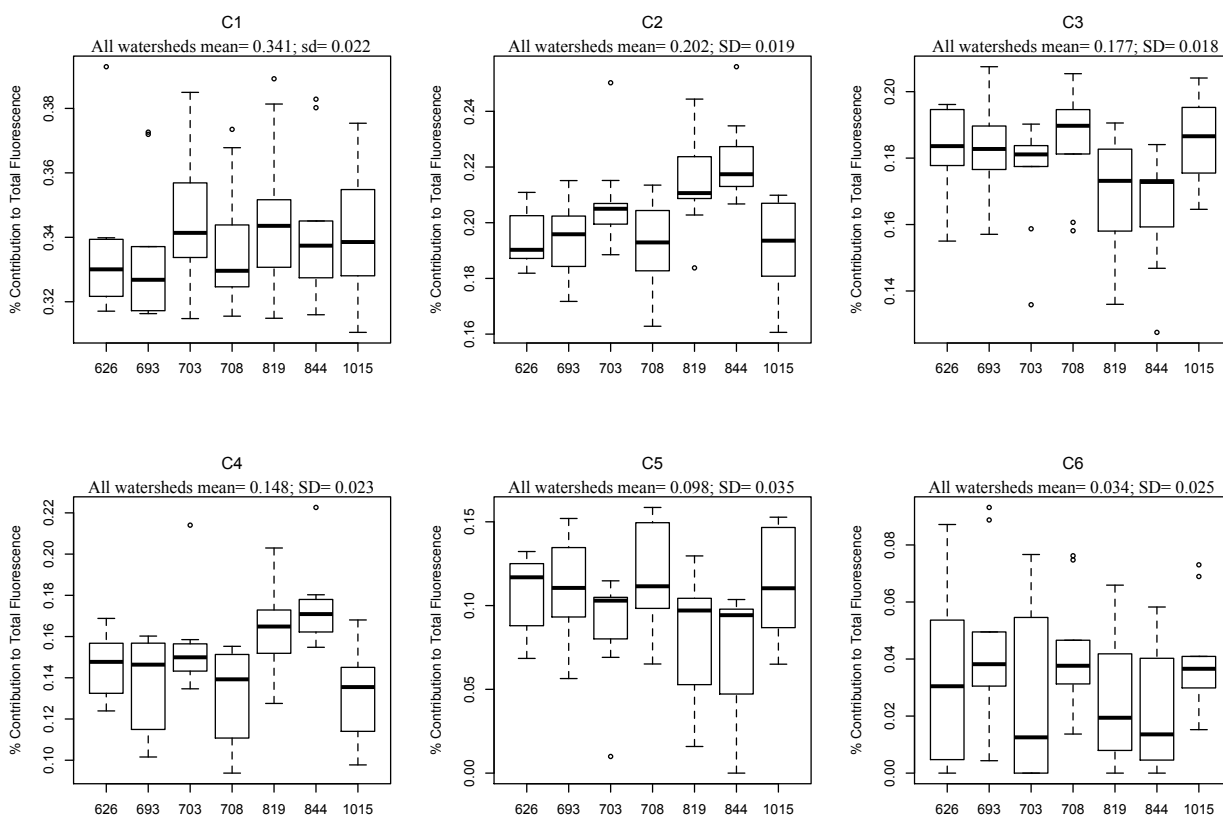
**Figure S4.3:** Split half validation plots for the six fluorescence components determined by PARAFAC analysis.

257

258



259  
 260 **Figure S4.4:** Box plots showing the percent contribution to total fluorescence from each of the  
 261 six components determined by PARAFAC analysis for each of the seven watersheds used in this  
 262 study. Means and standard deviations for each component summed across all watersheds is  
 263 included at the top of each panel.  
 264



265  
266  
267  
268  
269  
270

**Table S4.1:** Locations of maximum fluorescence values and the corresponding excitation and emission wavelengths for each of the six peaks (components) determined with PARAFAC modelling.

Component	Excitation (nm)	Excitation $F_{\max}$	Emission (nm)	Emission $F_{\max}$
1	315	0.2502	436	0.1688
2	270	0.2607	484	0.1422
	380	0.2539		
3	270	0.4125	478	0.1212
4	305	0.2648	522	0.1504
	435	0.1512		
5	325	0.1408	442	0.1321
6	285	0.3108	338	0.2350

271  
272

273 **Table S4.2:** Pearson correlation coefficients for PARAFAC components represented as percent  
 274 contribution to total fluorescence. Symbols “\*\*\*”, “\*”, represent p-values <0.001 and 0.001,  
 275 respectively.  
 276

	C1	C2	C3	C4	C5	C6
C1	1	0.55 **	-0.45 **	0.38 *	-0.66 **	-0.47 **
C2	-	1	-0.78 **	0.95 **	-0.90 **	-0.46 **
C3	-	-	1	-0.81 **	0.93 **	-0.13
C4	-	-	-	1	-0.87 **	-0.34 *
C5	-	-	-	-	1	0.16
C6	-	-	-	-	-	1

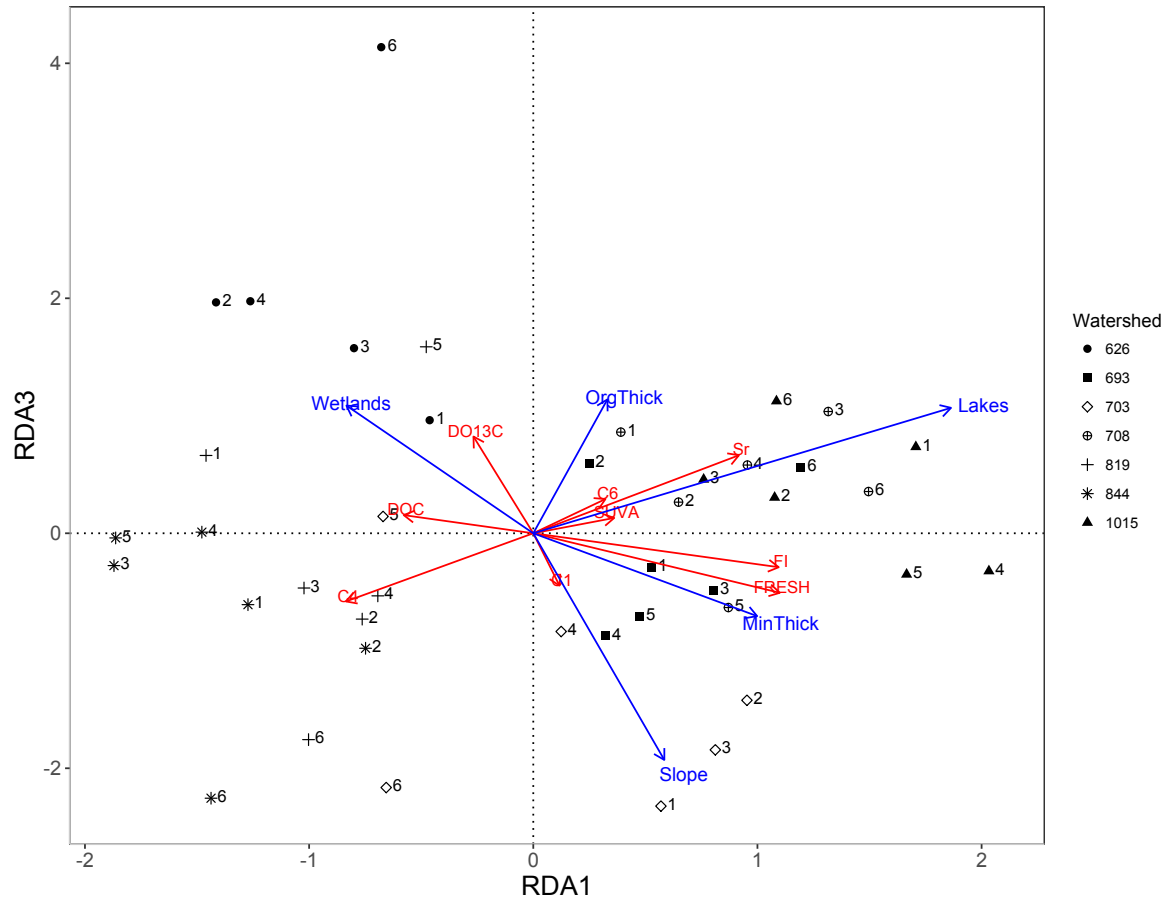
277

278

279 **S5. Redundancy analysis: Relationships between watershed characteristics and DOC**  
 280 **exports**

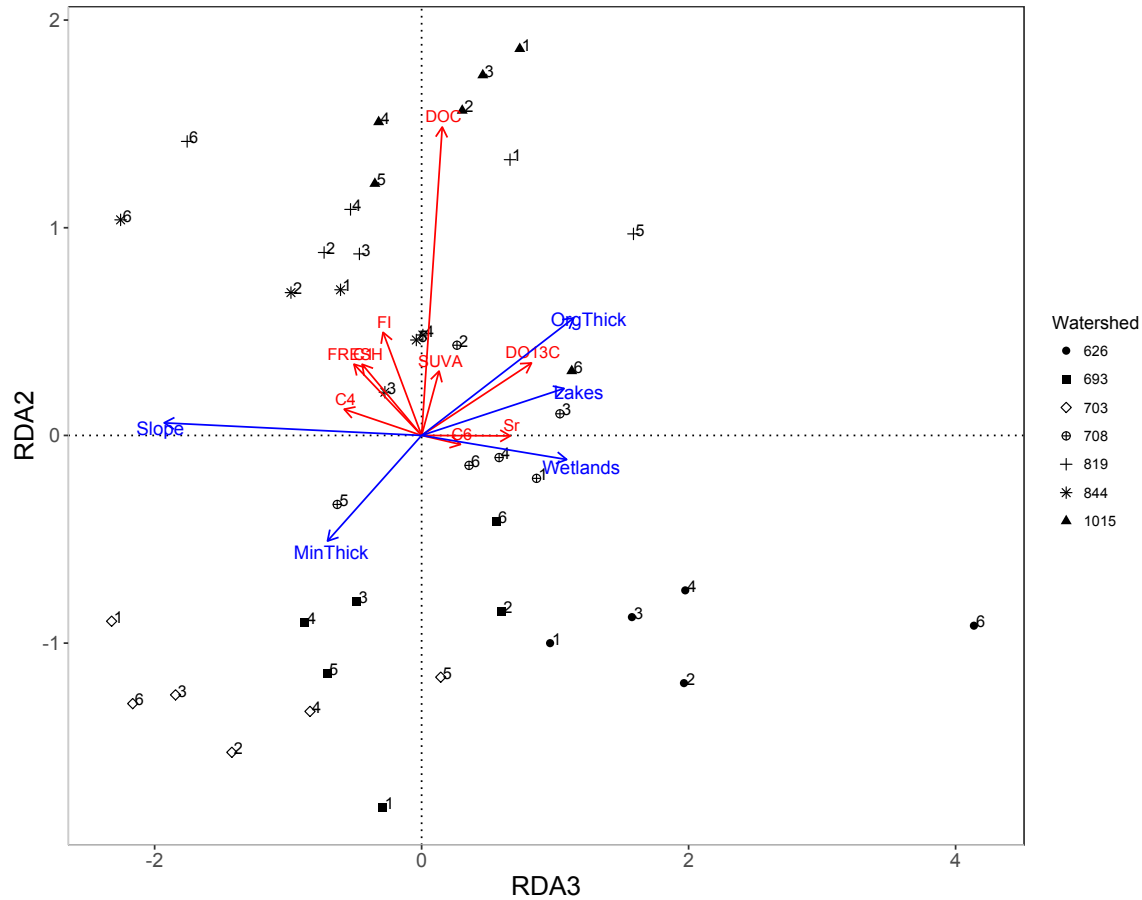
281

282 **Figure S5.1:** Partial-RDA Axis 1 versus Axis 3. RDA was performed under type 2 scaling.



283  
284  
285

**Figure S5.2:** Partial-RDA Axis 2 versus Axis 3. RDA was performed under type 2 scaling.



286  
287  
288

**Table S5.3:** Relative eigenvalues and the statistical significance of each axes in the partial-RDA.

Axis	Eigen -value	F marginal	F forward	P- marginal	P- forward	% total variance in Y	% total variance explained by all axis
1	1.420	18.717	11.047	0.0001	0.0001	15.78	47.3
2	0.902	11.887	9.158	0.0001	0.0001	10.02	30.1
3	0.654	8.622	8.531	0.0002	0.0002	7.27	21.8
4	0.013	0.175	0.175	1.0000	1.0000	0.15	0.4
5	0.011	0.143	0.143	0.9965	0.9965	0.12	0.4

289  
290  
291  
292

**Table S5.4:** Results of permutation test on the marginal effects of terms given under the reduced RDA model.

	df	Variance	F	Pr (>F)
Lakes	1	1.093	6.4789	0.001
Slope	1	0.5722	3.392	0.005
Wetlands	1	0.1207	0.7153	0.651
MinSoil	1	0.8403	4.9807	0.001
OrgSoil	1	0.6937	4.1118	0.001
Residual	34	5.7359		

293

294 **Table S5.5:** Biplot scores for partial-RDA axes using type 2 scaling.  
 295

	Axis1	Axis2	Axis3	Axis4	Axis5
Lakes	0.8471	0.1028	0.4853	-0.1871	0.0349
Slope	0.2658	0.0275	-0.8769	-0.0410	0.3825
Wetlands	-0.3789	-0.0527	0.4940	0.4033	-0.6664
MinSoil	0.4540	-0.2311	-0.3205	0.1128	0.7905
OrgSoil	0.1503	0.2569	0.5178	0.3138	0.7341

296

297 **Table S5.6:** Standardized coefficients for variables included in the partial-RDA using type 2  
 298 scaling. Coefficients represent the length of the vector in relation to the given axis and its relative  
 299 contribution to that axis.  
 300

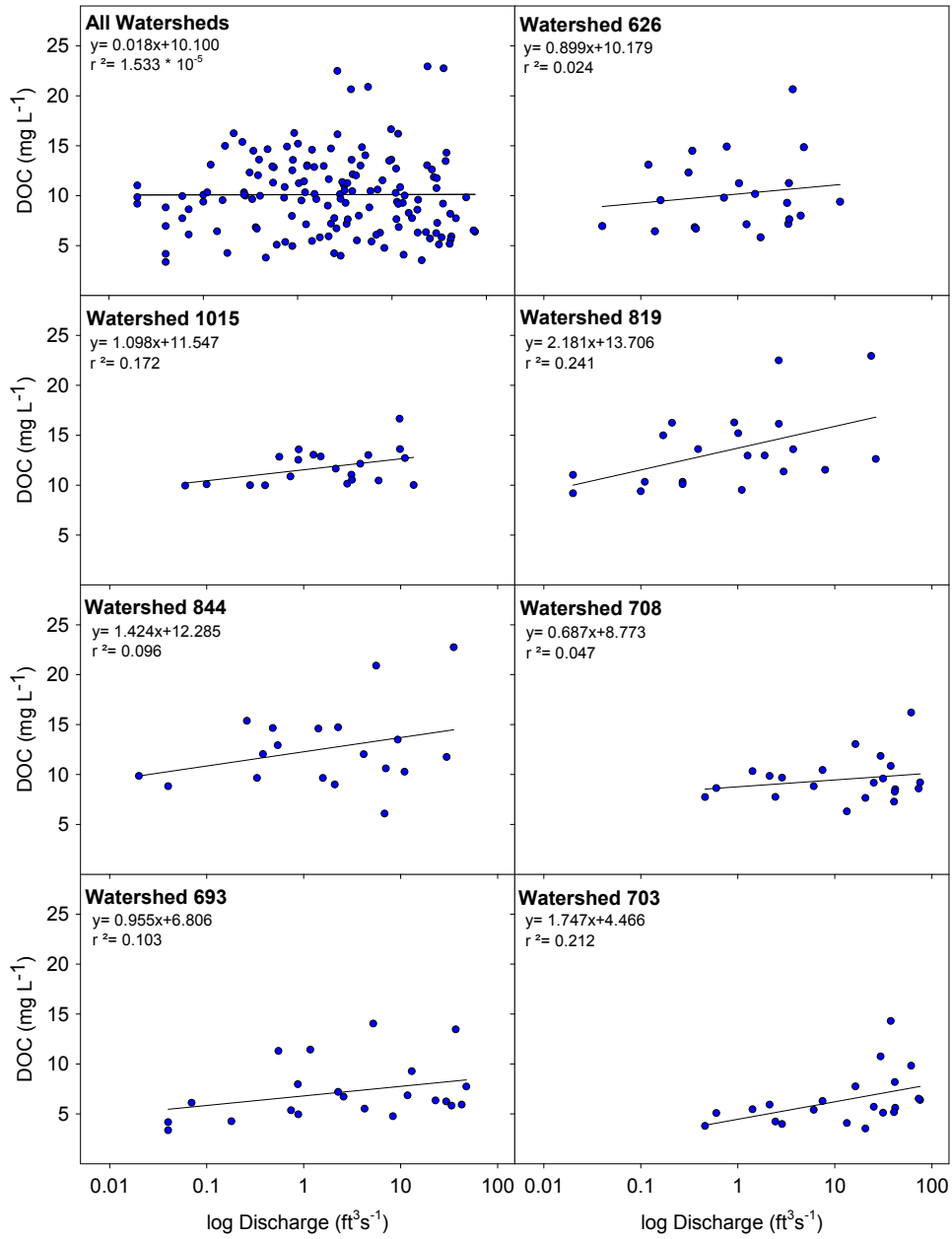
	Axis1	Axis2	Axis3	Axis4	Axis5
DOC	0.10308	0.78375	0.79112	0.79174	0.79204
DO13C	0.02198	0.05953	0.26876	0.27104	0.27141
Sr	0.25971	0.25971	0.39575	0.39901	0.39921
FI	0.37008	0.44613	0.47187	0.47188	0.47616
SUVA	0.04024	0.06987	0.07513	0.07548	0.07560
FRESH	0.37330	0.40960	0.48886	0.48886	0.49153
C1	0.00422	0.04047	0.10175	0.10612	0.10622
C4	0.21552	0.22043	0.32432	0.32674	0.32701
C6	0.03199	0.03257	0.05873	0.05873	0.06128

301

302 **S6. Evaluating relationships in DOC concentration and DOM character with stream**  
 303 **discharge and temperature**

304

305 **Figure S6.1:** Linear regressions of discharge versus DOC concentration for all watersheds (n=  
 306 158) combined and for each individual watershed (n= 21 for watersheds 703, 708, 819; n= 23 for  
 307 watersheds 626, 693, 844, 1015) included in our study for each watershed).



309 **Table S6.1:** Results of linear mixed effects models used to evaluate the relationship between DOC concentration or proxies of DOM  
 310 character with stream discharge and stream temperature. Random effects are displayed using the format “Random (random slope |  
 311 random intercept)”, where “~” indicates no random slope was included in the model. P-values significant at the 95% confidence level  
 312 are presented in bold.  
 313

Variable	Model	df	RMSE	Intercept	Fixed Effects			Conditional R <sup>2</sup>	Marginal R <sup>2</sup>
					log Q	Temp	logQ * Temp		
DOC	$b_1(\log Q) + b_2(\text{Temp}) + \text{Random}(\log Q   \text{Watershed})$	136	3.51	8.27 SE= 1.33	$b_1= 0.613$ SE= 0.131 t= 4.68 <b>p&lt; 0.001</b>	$b_2= 0.162$ SE= 0.063 t= 2.59 <b>p= 0.0107</b>	-	0.574	0.087
$\delta^{13}\text{C-DOC}$	$b_1(\log Q) + b_2(\text{Temp}) + \text{Random}(\log Q   \text{Watershed})$	133	0.324	-26.31 SE= 0.104	$b_1= -0.049$ SE= 0.131 t= -2.49 <b>p= 0.014</b>	$b_2= -0.024$ SE= 0.007 t= -3.50 <b>p&lt; 0.001</b>	-	0.353	0.096
$S_R$	$b_1(\log Q) + b_2(\text{Temp}) + b_3(\log Q * \text{Temp}) + \text{Random}(\text{Temp}   \text{Watershed})$	121	0.030	0.808 SE= 0.014	$b_1= -0.026$ SE= 0.004 t= -6.92 <b>p&lt; 0.001</b>	$b_2= -0.0013$ SE= 0.0009 t= -1.32 p= 0.186	$b_3= 0.0015$ SE= 0.0003 t= 5.29 <b>p&lt; 0.001</b>	0.621	0.288
SUVA <sub>254</sub>	$b_1(\log Q) + b_2(\text{Temp}) + \text{Random}(-   \text{Watershed})$	111	0.513	4.50 SE= 0.129	$b_1= 0.033$ SE= 0.026 t= 1.27 p= 0.206	$b_2= -0.011$ SE= 0.012 t= -0.919 p= 0.3603	-	0.072	0.041
Fluorescence Index	$b_1(\log Q) + b_2(\text{Temp}) + \text{Random}(-   \text{Watershed})$	25	0.030	1.37 SE= 0.017	$b_1= -0.009$ SE= 0.005 t= -1.76 p= 0.090	$b_2= 0.0002$ SE= 0.002 t= 0.106 p= 0.916	-	0.702	0.083
Freshness Index	$b_1(\log Q) + b_2(\text{Temp}) + \text{Random}(-   \text{Watershed})$	25	0.018	0.470 SE= 0.010	$b_1= 0.004$ SE= 0.003 t= 1.25 p= 0.223	$b_2= -0.003$ SE= 0.001 t= -2.91 <b>p= 0.008</b>	-	0.589	0.234

314

315 **Table S6.2:** Results of linear mixed effects models used to evaluate the relationship of PARAFAC components C1- C6 with stream  
 316 discharge and stream temperature. Random effects are displayed using the format “Random (random slope | random intercept)”,  
 317 where “~” indicates no random slope was included in the model. P-values significant at the 95% confidence level are presented in  
 318 bold.  
 319

Variable	Model	df	RMSE	Intercept	Fixed Effects			Conditional R <sup>2</sup>	Marginal R <sup>2</sup>
					log Q	Temp	logQ * Temp		
C1	$b_1(\log Q) + b_2(\text{Temp}) + \text{Random}(\sim   \text{Watershed})$	25	0.0109	0.344 SE= 0.005	$b_1 = -0.002$ SE= 0.002 $t = -1.03$ p= 0.315	$b_2 = 0.001$ SE= 0.001 $t = 1.99$ <b>p= 0.050</b>	-	0.276	0.275
C2	$b_1(\log Q) + b_2(\text{Temp}) + \text{Random}(\sim   \text{Watershed})$	25	0.0110	0.209 SE= 0.006	$b_1 = -0.005$ SE= 0.002 $t = -2.44$ <b>p= 0.022</b>	$b_2 = 0.0003$ SE= 0.0007 $t = 0.42125$ p= 0.677	-	0.414	0.204
C3	$b_1(\log Q) + b_2(\text{Temp}) + \text{Random}(\sim   \text{Watershed})$	25	0.0112	0.183 SE= 0.006	$b_1 = 0.006$ SE= 0.002 $t = 3.278$ <b>p= 0.003</b>	$b_2 = -0.003$ SE= 0.001 $t = -3.26$ <b>p= 0.003</b>	-	0.529	0.420
C4	$b_1(\log Q) + b_2(\text{Temp}) + \text{Random}(\sim   \text{Watershed})$	25	0.0132	0.143 SE= 0.007	$b_1 = -0.008$ SE= 0.002 $t = -3.39$ <b>p= 0.002</b>	$b_2 = 0.003$ SE= 0.001 $t = 4.26$ <b>p&lt; 0.001</b>	-	0.690	0.457
C5	$b_1(\log Q) + b_2(\text{Temp}) + \text{Random}(\sim   \text{Watershed})$	25	0.0213	0.103 SE= 0.011	$b_1 = 0.011$ SE= 0.003 $t = 3.07$ <b>p= 0.005</b>	$b_2 = -0.003$ SE= 0.001 $t = -2.36$ <b>p= 0.027</b>	-	0.453	0.331
C6	$b_1(\log Q) + b_2(\text{Temp}) + \text{Random}(\sim   \text{Watershed})$	25	0.0234	0.006 SE= 0.012	$b_1 = -0.002$ SE= 0.003 $t = -0.55$ p= 0.585	$b_2 = 0.005$ SE= 0.002 $t = 3.12$ <b>p= 0.005</b>	-	0.380	0.379

321

322 **References**

323 Banner, A., MacKenzie, W., Haeussler, S., Thomson, S., Pojar, J., Trowbridge, R.: A field guide  
324 to site identification and interpretation for the Prince Rupert forest region, Handbook 26, Res.  
325 Br., British Columbia Ministry Forests, Victoria, British Columbia, 42 pp., 1993.

326

327 Cohn, T.A., Kiang, J.E., Mason, Jr., R.R.: Estimating Discharge Measurement Uncertainty Using  
328 the Interpolated Variance Estimator, American Society of Civil Engineers,  
329 doi:10.1061/(ASCE)HY.1943-7900.0000695, 2013.

330

331 Floyd, W.C., Korver, M.C., Owen, C., McPhail, J., Brunsting, R., van Meerveld, I.: Stage-  
332 discharge time series- Calvert Island, Hakai Institute, doi:dx.doi.org/10.21966/1.243102, 2016.

333

334 Giesbrecht, I., Banner, A., Hoffman, K., Sanborn, P., Saunders, S., MacKinnon A.: Ecosystem  
335 comparison plots- Calvert Island, Hakai Institute, doi:dx.doi.org/10.21966/1.56481, 2016.

336

337 Gonzalez Arriola S., Frazer, G.W., Giesbrecht, I.: LiDAR-derived watersheds and their metrics  
338 for Calvert Island, Hakai Institute, doi:dx.doi.org/10.21966/1.15311, 2015.

339

340 Green, R.N.: Reconnaissance level terrestrial ecosystem mapping of priority landscape units of  
341 the coast EBM planning area: Phase 3, Prepared for British Columbia Ministry Forests, Lands  
342 and Natural Resource Ops., Blackwell and Associates, Vancouver, Canada, 2014.

343

344 Herschy, R.: The analysis of uncertainties in the stage-discharge relation, Flow Meas. Instrum.,  
345 5, 188-190, 1994.

346

347 Howes, D.E., and Kenk, E.: Terrain classification system for British Columbia, MOE Manual 10,  
348 2, Province of British Columbia Ministry Environment and Ministry of Crown Lands, Victoria,  
349 Canada, 102 pp., 1997.

350

351 ISO: Liquid flow measurement in open channels - velocity-area methods, Technical Report 772,  
352 International Organization for Standardization, Geneva, Switzerland, available at: www.iso.org,  
353 1979.

354

355 ISO Standard 9196: Liquid flow measurement in open channels - Flow measurements under ice  
356 conditions, International Organization for Standardization, Geneva, Switzerland, available at:  
357 www.iso.org, 1992.

358

359 ISO Standard 748: Hydrometry - Measurement of liquid flow in open channels using current-  
360 meters or floats, International Organization for Standardization, www.iso.org, 2007.

361

362 LMFIT Development Team: Lmfit, Least-squares Minimization with Bounds and Constraints,  
363 version 0.8.3, available at: <http://lmfit.github.io/lmfit-py/>, 2015.

364

365 MacKenzie, W.H., Moran, J.R.: Wetlands of British Columbia: a guide to identification, Land  
366 Manage. Handb. No. 52., Res. Br., British Columbia Ministry Forests, 287 pp., 2004.  
367  
368 Minasny, B., and McBratney, A.B.: A conditioned Latin hypercube method for sampling in the  
369 presence of ancillary information, *Comput. Geosci.*, 32, 1378-1388, 2006.  
370  
371 Moore, R.D.: Introduction to salt dilution gauging for streamflow measurement Part I,  
372 *Streamline Watershed Management Bulletin*, 7, 20-23, 2004a.  
373  
374 Moore, R.D.: Introduction to salt dilution gauging for streamflow measurement Part II, constant-  
375 rate injection, *Streamline Watershed Management Bulletin*, 8, 11-15, 2004b.  
376  
377 Moore, R.D.: Introduction to salt dilution gauging for streamflow measurement Part III, slug  
378 injection using salt in solution, *Streamline Watershed Management Bulletin* 8, 1-6. 2005.  
379  
380 Scarpone, C., Schmidt, M.G., Bulmer, C., and Knudby, A.: Modelling soil thickness in the  
381 critical zone for Southern British Columbia, *Geoderma*, 282:59-69, 2016.  
382  
383 Soil Classification Working Group: The Canadian system of soil classification, 3, Publication  
384 1646, Agriculture and Agri-Food, Canada, 187 pp., 1997.  
385  
386 Sontek/YSI: Flowtracker Handheld ADV Technical Manual, Firmware Version 3.3, Software  
387 Version 2.20, 2007.